Preliminary investigation of seismic velocity variation at the Rotokawa and Ngatamariki Geothermal Fields

Steven Sewell[1], Martha Savage[1], John Townend[1], Stephen Bannister[2], Lawrence Hutchings[3]

[1]Victoria University, Room 503, Cotton Building, Wellington, 6140

[2]GNS Science, Avalon, PO Box 30-368, Lower Hutt, 5040

[3]Lawrence Berkeley National Laboratory, One Cyclotron Road, Berkeley, California, 94720

Steven.Sewell@vuw.ac.nz

Keywords: *Ngatamariki, Rotokawa, seismic velocity*

ABSTRACT

Imaging of seismic properties has the potential to provide important information on the physical and thermodynamic properties of rocks and their pore fluids within and adjacent to geothermal reservoirs. Obtaining accurate seismic velocity models is also important for reducing uncertainty in microseismic event locations, particularly for event depths. As part of a preliminary investigation into seismic property variations at the Rotokawa and Ngatamariki geothermal fields, we have completed a first-pass interpretation of well logging data and preliminary 1D and 3D seismic tomography inversions. The well logs show a large contrast in P-wave velocity (~1 km/s) for the Tahorakuri Formation between NM9 in the north and NM10 in the south of the Ngatamariki field. This contrast appears to be related mostly to a reduction in matrix porosity in NM9 for the Tahorakuri Formation (~10% lower in NM9) as shown by the neutron porosity logs. To investigate the cause of the difference in matrix porosity, bulk rock chemistry measurements were made on drill cuttings in NM9 and NM10 at 5m depth spacing using portable XRF. The portable XRF measurements show an increase in silica concentration of ~10-20% for the Tahorakuri Formation in NM9. It therefore appears that silicification of the Tahorakuri Formation in the north of the field, formed by intense relict magmatic-hydrothermal alteration above an intrusive, has lowered the matrix porosity and increased seismic velocity in the vicinity of NM9. As the northern wells at Ngatamariki generally have low permeability through the Tahorakuri Formation, imaging the high seismic velocity zone using seismic tomography offers a potential way to map the low permeability in 3D. Preliminary seismic tomography has been conducted utilizing a Monte Carlo 1D inversion using the VELEST code and 3D inversion using the Simul code. This has shown that a high to low P-wave velocity contrast (~0.5-1 km/s) occurs in the north-northwest of the Ngatamariki field that may be due to the silicification above the intrusive. This contrast appears to strike approximately NNE-SSW through NM9, suggesting that the silicification of the Tahorakuri Formation, and hence low permeability, does not continue east of this well. However, synthetic Simul tests show that the spatial resolution of the current seismometer array is generally poor. In order to improve the spatial resolution, an expanded array of 30 additional seismometers was installed in February 2017 which will record for a year.

1. INTRODUCTION

1.1 Seismic velocity in geothermal fields

Seismic velocity (P-wave, Vp and S-wave velocity, Vs), is known to vary due to both formation properties (matrix porosity, lithology, alteration, permeability/fracturing e.g. Wyering et al., 2014) and the thermodynamic properties of the fluids within the pore space (temperature, pressure, phase (water/gas/steam) e.g. Jaya et al., 2010). Therefore, seismic velocity imaging via tomographic inversion has the potential to provide useful information on geothermal reservoirs.

The absolute accuracy with which microseismic event locations can be determined is also dependent upon the accurate knowledge of seismic velocity variations. The path which seismic energy takes from an earthquake source to a seismometer is determined by the seismic velocity of the rock through which it travels (e.g. Rawlinson et al., 2010). Uncertainty in velocity models therefore leads to uncertainty in hypocentre locations, particularly for event depths. Determining seismic velocity is therefore also important for obtaining accurate microseismic event locations which can then be used for interpreting major structures and injection fluid movement within geothermal fields (e.g. Sewell et al., 2015).

1.2 The Ngatamariki and Rotokawa Geothermal Fields

The Ngatamariki and Rotokawa Geothermal fields are high temperature geothermal fields on the North Island of New Zealand (Figure 1). Electricity generation on the Rotokawa field began in 1997 with a small binary power plant (34 MWe) and in 2010 a second 138 MWe triple flash power plant was installed bringing the total installed capacity to 172 MWe. A microseismic monitoring array of 10 seismometers has been operating at Rotokawa since mid-2008. Sewell et al., (2015) and Sherburn et al., (2015) outline how this monitoring has been useful for characterizing injection fluid flow and large-scale permeability within the reservoir. Production on the Ngatamariki field began in 2013 with the commissioning of an 83 MWe binary plant. Nearly 100% of the produced fluid at Ngatamariki is injected in two locations ~1.5 km north and south of production wells (Figure 1). A microseismic monitoring network has operated at Ngatamariki since mid-2012 that consists of nine surface seismometers and three downhole seismometers installed in monitoring wells between 300-500m depth. In order to better constrain the velocity model for the field, and hence microseismic event depths, a checkshot survey was performed on one well in the north of the field. Sonic logs

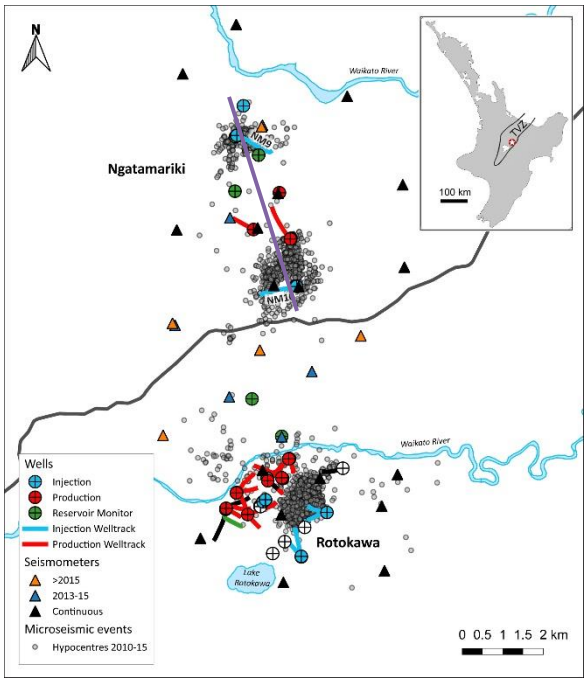

Figure 1: Map of the Rotokawa and Ngatamariki geothermal fields showing production and injection well tracks and seismometers active during the 2012-2015 period. Hypocentres (grey dots) from manually picked P and S arrivals and double-difference relocation from GNS Science over the period are also shown. The inset shows the location of the fields (red star) within the Taupo Volcanic Zone (TVZ) in the North Island of New Zealand. The purple line shows the location of the cross-section in Figure 2.

were also collected on a number of wells as part of a broader wireline logging program (Wallis et al., 2009).

1.2 The Ngatamariki and Rotokawa Geothermal Fields

The fields are located within the central Taupo Volcanic Zone (TVZ) on the eastern margin of the TVZ rift. The upper 1 km of the fields consists of surficial deposits (loosely compacted pumice and sediments), the Huka Falls Formation (lacustrine mudstones, siltstones and sandstones), rhyolites, the Waiora Formation (volcaniclastic sediments) and the Whakamaru group ignimbrite (also known as the Wairakei Ignimbrite) (Figure 2).

Below the Whakamaru Ignimbrite is the Tahorakuri Formation, which consists mostly of interlayered tuffs and volcaniclastic sediments with minor intervals of ignimbrites, rhyolites and basaltic to andesitic lavas, dykes and breccias. The Tahorakuri Formation lies between approximately 1 and 2 km bsl at Ngatamariki and is the main formation of the reservoir. Below the Tahorakuri in the south of the Ngatamariki field, and throughout Rotokawa, is an ~1 km thick andesitic sequence (dominantly lavas and breccias). Permeable zones for production wells at Rotokawa mostly occur in these andesite lava layers which are up to 1.5 km thick in the production area. Beneath the andesite is greywacke which is the basement rock of the TVZ (Mesozoic age). This been intersected in one well in the south of the Ngatamariki field at 3 km bsl in NM6 (Figure 2) and is the main injection formation at Rotokawa where it is intersected at ~1.5-2 km bsl.

Alteration above 1 km bsl is variable, but often includes relatively high smectite and smectite-illite clay, particularly in the south of the Ngatamariki field (Boseley et al., 2010; Chambefort et al., 2016a). Alteration below 1 km bsl within the reservoirs is dominantly propylitic (mainly illite, chlorite, epidote and quartz) for most of the fields.

A unique feature of the Ngatamariki field is the intrusive complex (diorite to tonalite in composition) in the north of the field and its associated magmatic-hydrothermal alteration halo that has been intersected in three of the wells (Chambefort et al., 2016a, 2016b). Age dating shows this intruded into the Tahorakuri Formation at ~0.65-0.71 Ma, before the Whakamaru Group ignimbrites (Chambefort et al., 2014). Alteration within the Tahorakuri Formation above the intrusive is generally intense ranging from potassic to advanced argillic and phyllic assemblages. Phyllic alteration is the most wide-spread of the alteration types and is typified by intense silicification, white mica and pyrite (Chambefort et al., 2016b). The wells drilled in this area, particularly NM4 and NM8, are generally lower permeability than the other wells at Ngatamariki. The temperature profiles of all three wells through the Tahorakuri Formation are linear with depth, indicating conductive heat flow and therefore low vertical permeability.

2. PRELIMINARY ASSESSMENT OF THE MAIN FACTORS CONTROLLING SEISMIC VELOCITY

Borehole compensated sonic logs were obtained in NM8, NM9 and NM10 as part of a suite of logs that generally included gamma, neutron porosity, resistivity, self-potential, density and formation imaging (FMI) logs (Wallis et al., 2009). A dipole sonic log was acquired in NM10 and hence Vs measurements are available for this well. The sonic logs measure seismic velocity at depth intervals of ~0.15 m and consequently the log captures the high variability in velocity (on average +/- 1 km/s but up to 3 km/s variation) at the sub metre scale (Figure 3). Taking the sliding average velocity with depth over ~10 m intervals reduces the variability significantly.

Portable XRF (pXRF) measurements were made on drill cuttings at 5 m depth intervals over the logging intervals in NM9 and NM10 to assist in identifying the effect that lithology and alteration has on seismic velocity (Figure 3). An Olympus DELTA premium was used which provides elemental abundances for elements heavier than aluminium to precision better than 1%.

The gamma log, which measures natural radioactivity due to the decay of K, U and Th, and the potassium measurements from the pXRF were used to correct the cuttings depths. As uranium and thorium values were below 15 ppm, the majority of the gamma response is from potassium. Cuttings depths were therefore corrected to obtain the best fit between the gamma and potassium values. Corrections were in places up to 30 m higher than the original calculated cuttings depths which appears to be due to zones of partial cuttings loss during drilling.

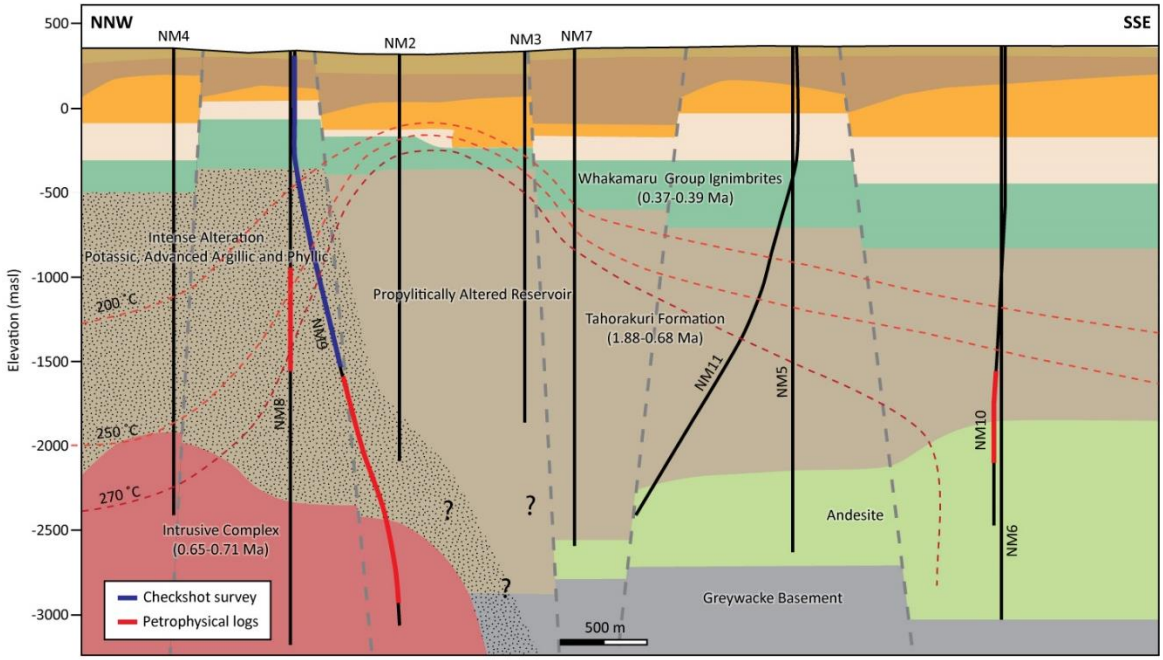

Figure 2. NNW-SSE cross-section through Ngatamariki showing the main geologic units, selected natural state isotherms and the area of intense magmatic-hyrdothermal alteration associated with the intrusive complex in the north of the field. Age dates shown in brackets are from Chambefort et al., 2014. Modified after Chambefort et al., 2016b and Boseley et al., 2010.

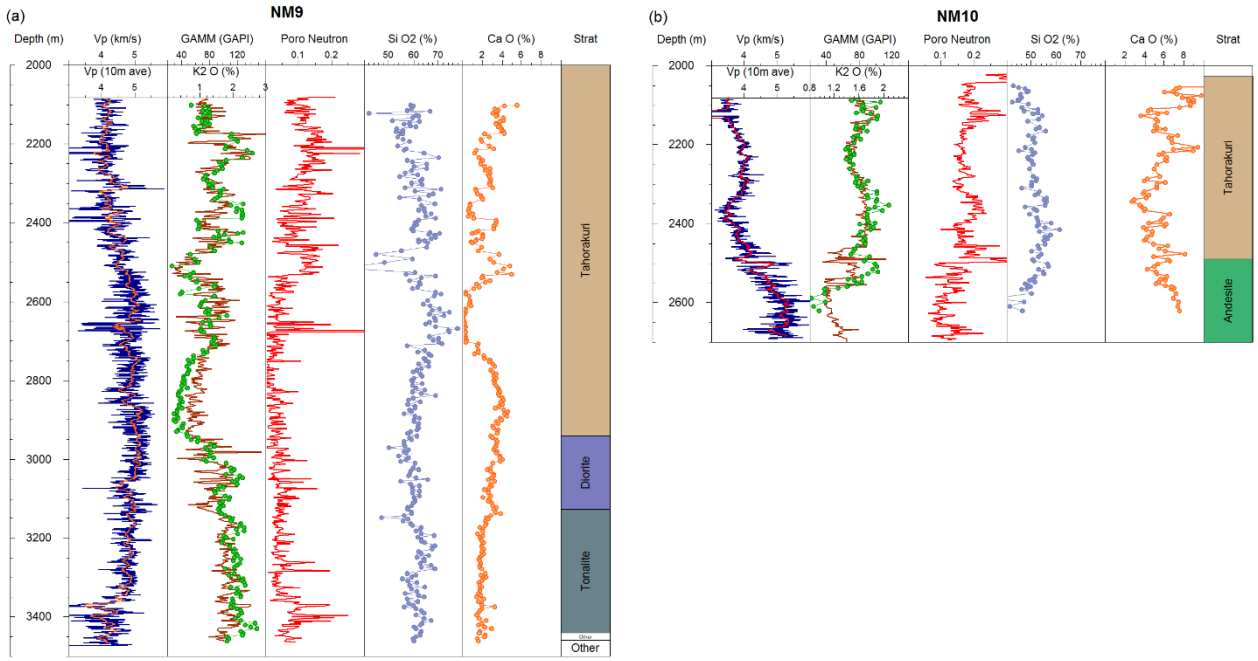

Figure 3. Vp (blue = original data, red = 10 m sliding average), gamma and neutron porosity logs from (a) NM9 and (b) NM10. Potassium (green dots overlain on the gamma log), silicon and calcium as determined from pXRF (converted to oxides) are also shown. Cuttings depths were adjusted to obtain an optimal fit to the gamma log.

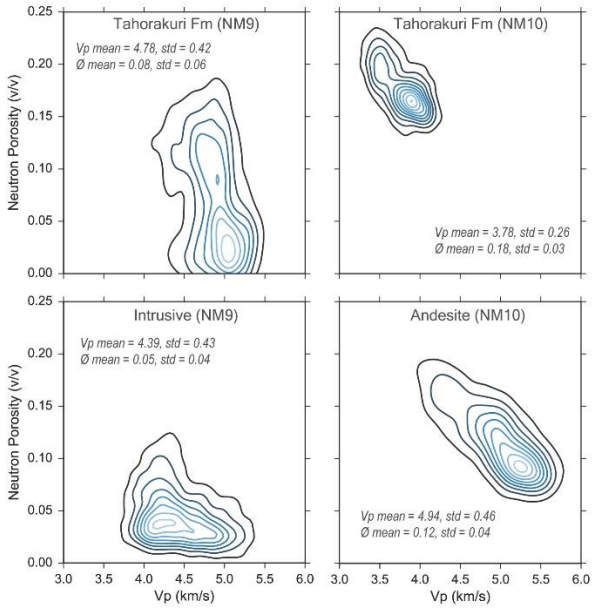

Figure 4. Vp versus neutron porosity for the Tahorakuri Formation and intrusive in NM9 and the Tahorakuri Formation and andesite in NM10.

2.2 The Ngatamariki and Rotokawa Geothermal Fields

The logs show clearly the relationship between matrix porosity, formation type and seismic velocity. Velocity in NM9 is on average, significantly higher than in NM10 for the Tahorakuri Formation (between 3.5-4 km/s for NM10 versus 4-5 km/s in NM9). Likewise, porosity, as measured by the neutron porosity log, for the Tahorakuri Formation is significantly different between the wells ranging from 0-15% (average of 8%) for NM9 versus 15-20% (average of 18%) for NM10. Velocity is particularly high (average of ~5 km/s) and porosity particularly low (average of ~ 2-3%) from ~2530 m depth to ~2940 m immediately above the intrusive complex in NM9.

The relationship between seismic velocity and porosity is well established in the oil and gas sector, where sonic logs are often used to calculate porosity. It is noted though that the neutron porosity log measures the total hydrogen ion content and therefore measures both water in pore spaces and clay-bound water. Quantitative XRD measurements are planned to assess the impact clay has on both the sonic and neutron logs.

2.3 Effect of intrusion-related silicification on seismic velocity

The ~1 km/s difference in Vp and ~10% difference in porosity between NM9 and NM10 for the Tahorakuri Formation appears to be due to silicification formed during the intense magmatic-hydrothermal alteration associated with the intrusive (**Error! Reference source not found.**). Silica concentrations in cuttings from the logging intervals are between 55-70% for NM9 compared with 45-55% for NM10. This appears to be related to intense alteration, particularly in-filling of pore-space by silica. The increase in velocity for NM9 however does not appear to be due to in-filling of pore space alone. Given the same rock type and reduction of pore space alone, the NM9 samples should plot along the same linear trend as the NM10 samples. **Error! Reference source not found.** shows this is not the case. The steeper slope of the NM9 samples suggests that the matrix of the rock has been stiffened, most likely by the replacement of softer minerals with silica and cementing of the matrix frame.

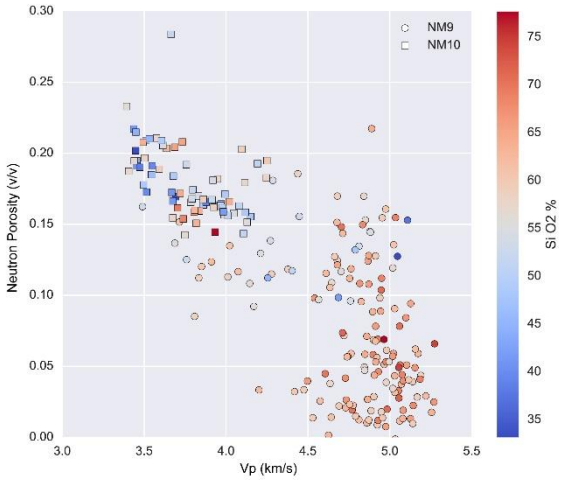

Figure 5. Vp versus neutron porosity for the Tahorakuri Formation. Porosity values are average log values +/- 2.5 m above and below the corrected cuttings depths. Color shows the silica concentrations as determined via pXRF.

3. SEISMIC TOMOGRAPHY

Seismic tomography has been a popular geophysical method for imaging seismic properties of the subsurface since the mid 1970's at all scales of investigation; global (>100 km's), lithospheric-crustal (10-100's of km's), local (<10 km) (e.g. Rawlinson et al., 2010; Rawlinson and Sambridge, 2003; Thurber and Ritsema, 2007). The term 'seismic tomography' is a somewhat generic term that is often used to describe a range of methods all with the common goal of determining spatial and temporal variations in the seismic properties of the subsurface. Both natural (e.g. earthquakes) and/or manmade (e.g. explosive charges, induced events) seismic sources can be used.

3.1. Arrival time dataset

The travel-time dataset for this preliminary work was obtained from manually picked P & S arrivals from 124 events that occurred in the three main clusters of seismicity (~50 events at Rotokawa, ~40 for southern Ngatamariki and ~30 for northern Ngatamariki) (**Error! Reference source not found.**). The picking procedure of Diehl and Kissling, (2009) was followed that includes making estimates of pick uncertainty (**Error! Reference source not found.**).

As tomographic inversion uses the RMS misfit criteria as part of the objective function, it is highly sensitive to outliers (i.e. arrivals with high misfit between the observed and calculated traveltimes - residuals, which is often due to inaccurate arrival time picks) (e.g. Rawlinson and Sambridge, 2003). Picks with anomalously high residuals were therefore removed from the dataset by iteratively removing those with residuals that were greater than 0.5s and greater than two standard deviations higher than the rest of the picks. This was repeated until little to no change in the overall RMS value was observed (removal of ~2% of picks). Events with high RMS residual values (~2-3 events)

and events with greater than 3 picks that were identified as outliers were manually reviewed and in most cases found to have low signal-to-noise picks which were removed.

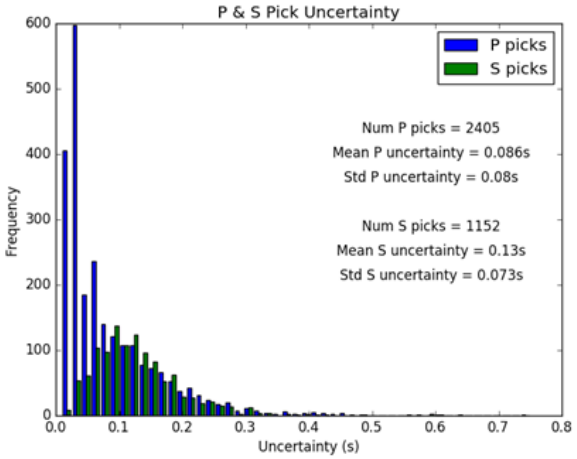

Figure 6. Distribution of P and S phase pick uncertainty for the 124 manually picked events across the Rotokawa and Ngatamariki network.

3.2. Monte Carlo VELEST – 1D velocity inversion

The VELEST seismic tomography code of Kissling et al., 1994 solves the coupled hypocentre-velocity problem for layered, one-dimensional velocity models. As the hypocentre-velocity problem is highly non-linear, regularization is used (damping in the case of VELEST) to linearize the problem and to find a local minimum to an objective function (for VELEST, solutions seek to minimise the RMS misfit between the observed and calculated travel-times). As the solution is a local minimum, it is highly dependent on the initial velocity model (i.e. the same fit to the data can be obtained from different starting and final velocity models). It is therefore important to test a range of starting models within the expected range of possible seismic velocities for the particular area.

The 1D model layer velocities obtained from VELEST will be approximately equal to the average velocity for the particular layer depth range (Kissling et al., 1994) over the region sampled by the ray-paths (i.e. in the region between events and stations). VELEST also solves for 'station correction' terms for each seismometer used in the inversion. These terms account for velocity variation from the 1D average velocity model (which includes local, shallow velocity structure and larger scale 3D velocity variation). The station correction terms can therefore provide an indication of relative 3D velocity variation within an area (i.e. which areas are on average higher velocity and which areas slower velocity).

3.2.1. Starting models

Six layers were used to approximate the broad-scale geologic layering within the field (**Error! Reference source not found.**a). Best-guess starting velocities for each layer were based on the NM9 checkshot, sonic logs and geology. The first layer approximates the shallow geology (loosely compacted surface sediments and pumice, Huka Falls formation lake sediments and rhyolite layers) and therefore has the lowest velocities. The next four layers cover the Wairakei Ignimbrite and Tahorakuri Formation. The top of the final layer is at the approximate depth of the contact between the Tahorakuri sediments and the Ngatamariki andesite and the intrusive (diorite/tonalite) in the north of the field.

A set of 1000 Vp starting models were generated using normally distributed random velocities for each layer using the best-guess P velocity model as the mean and standard deviations of +/- 1 km/s for each layer with all velocities constrained to be greater than 0.5 km/s (**Error! Reference source not found.**a). The generated velocity distribution for each layer covers the range of velocities measured within the field. S velocity models were generated from the P velocity models using a Vp/Vs ratio of 1.75 (based on the average measured Vp/Vs from a dipole sonic log in NM8) (**Error! Reference source not found.**c).

3.2.2. Final models

All 1000 models were successfully run to completion with nine iterations of hypocenter-velocity adjustment. The final RMS values obtained for all models were below 0.1 s, which is approximately the uncertainty in the arrival time data (**Error! Reference source not found.**). Overall the final P velocity model distributions show a large range of seismic velocities, with variation of at least +/-1 km/s (+/- 20%) for Vp and +/- 0.5 km/s (+/- 20%) for Vs for most layers (**Error! Reference source not found.**b and 8d). In general, velocities were lowered from the starting model velocities, particularly between 1 to 2 km bsl. The upper-most and lower-most layer velocity distributions were only slightly changed from their starting distributions, which likely reflects the lack of constraints for these layers (due to event depths being between 1.5 to 3.5 km bsl). Final P velocities between 1 and 2 km bsl were mostly slower than the measured velocities from NM9 at the same depths (**Error! Reference source not found.**).

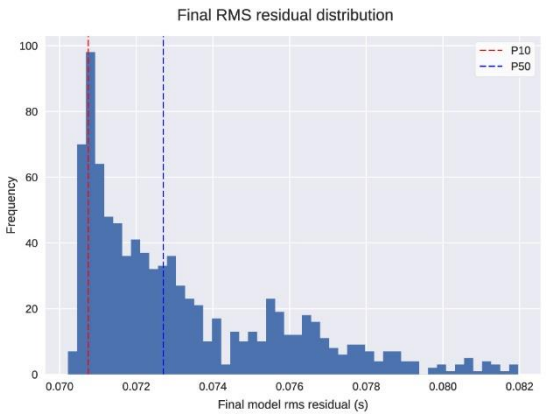

Figure 7. Final RMS distribution for all 1000 models after nine iterations. Lower RMS = closer fit between observed and calculated traveltimes from VELEST. The dashed red and blue lines show the location of the 10th and 50th (mean) percentile RMS values respectively.

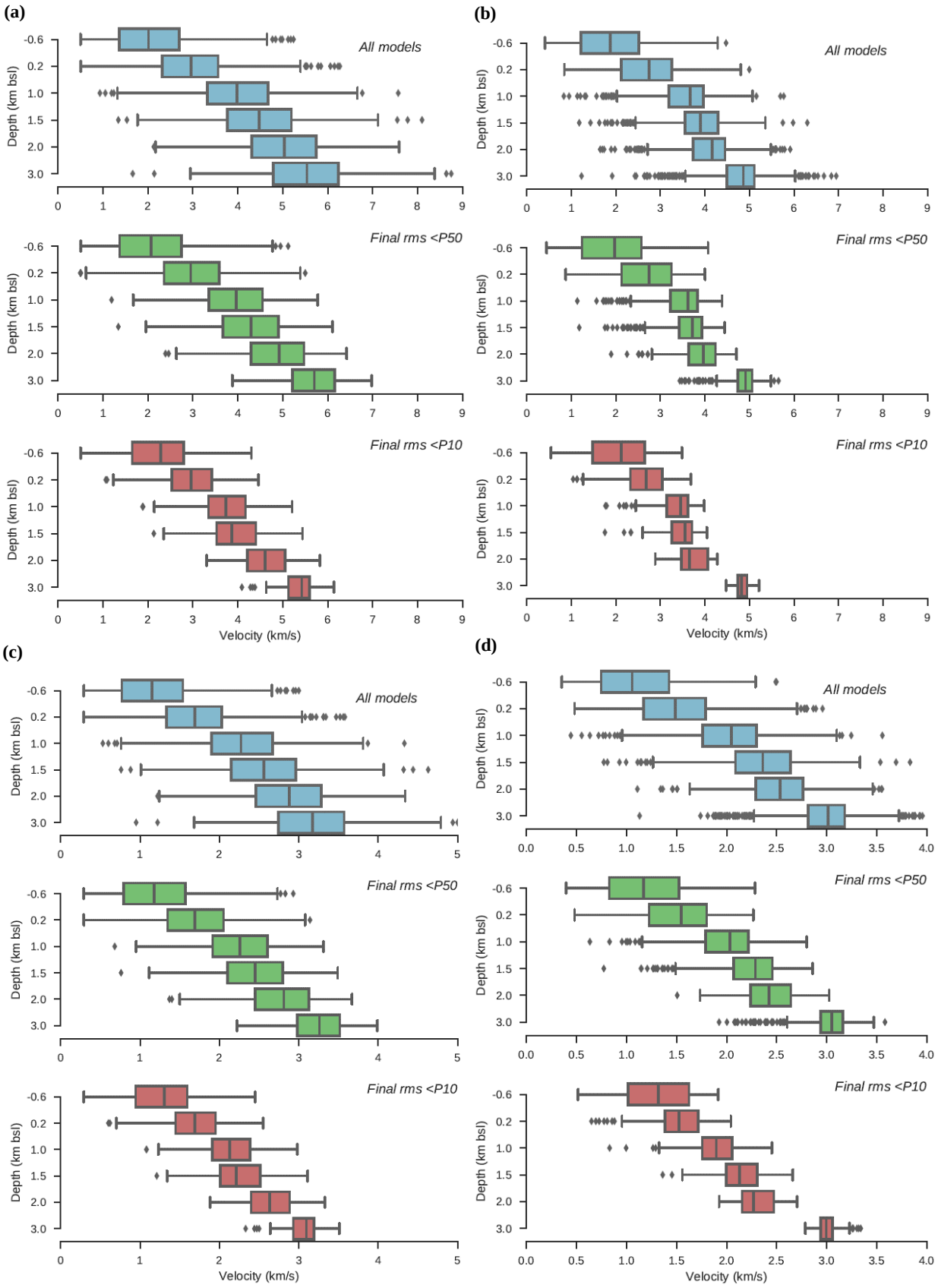

Figure 8. (a) starting Vp models (b) final Vp models, (c) starting Vs models and (d) final Vs models for the Monte Carlo VELEST. Models with final rms values below the P10 (i.e. top 10% best-fitting models) and below the P50 values are shown for each.

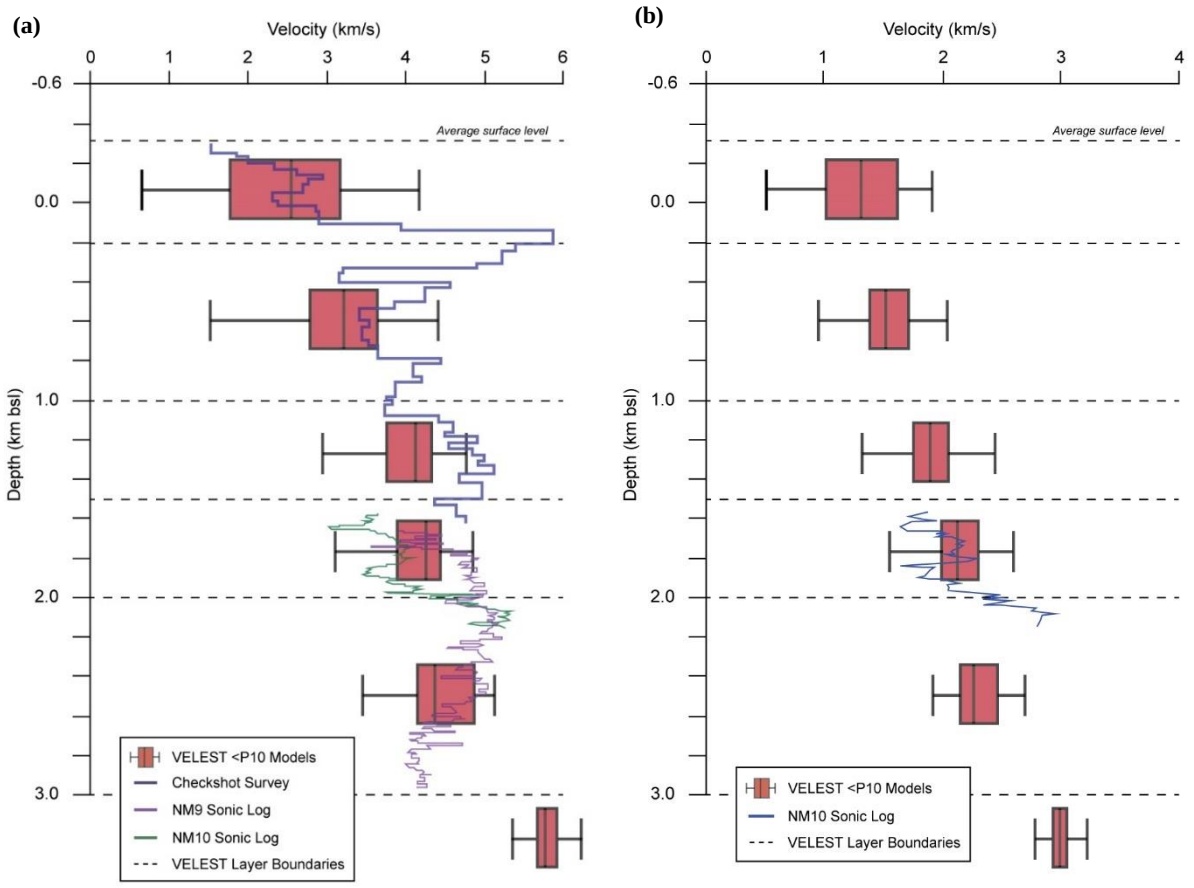

Figure 9. Comparison between the best-fitting (rms values < P10) for (a) Vp and (b) Vs and measured velocities from the checkshot and NM9 and NM10 sonic logs.

3.2.3. Station Corrections

VELEST also solves for 'station correction' terms for each seismometer used in the inversion. These terms account for velocity variation from the 1D average velocity model (which includes local, shallow velocity structure and larger scale 3D velocity variation). The station correction terms can therefore provide an indication of relative 3D velocity variation within an area (i.e. which areas are on average higher velocity and which areas slower velocity).

Error! Reference source not found. shows the average station correction terms derived from all 1000 models. The correction terms are relative to NS13 which is close to the centre of the array and has operated for most of the 2012-13 period. The Vp station corrections are negative in the north and west suggesting, on average, faster velocities in these areas. Positive values are observed for the eastern stations suggesting, on average, slower P velocities. The Vs station corrections, show negative values for Ngatamariki in the NW and in the NW of Rotokawa, suggesting faster Vs in these areas, whilst large positive values are observed in the east for Ngatamariki, and for one station in the east at Rotokawa, suggesting slower Vs in these areas.

3.3. 3D VELOCITY INVERSION

A preliminary 3D seismic tomography (Vp and Vs) inversion for the combined Rotokawa and Ngatamariki was obtained utilising the Simul code of Thurber (1983). The 3D inversions used the same traveltime dataset as the VELEST inversions. The pick uncertainties were used to weight data in the 3D inversion (i.e. if uncertainty was in the top 10% lowest uncertainties then the weight was assigned 1.0, if in the top 25% then the weight was 0.75, if 50% then the weight was 0.5, if 75% then weight was 0.25 and if 90% then the weight was 0.1).

3.1. Starting models

Three initial models were considered, a 1D model based on the checkshot and sonic logs from NM9, a 1D model based on the average of the Monte Carlo VELEST models and a 3D model based on the geology. The 3D starting model approximates the large-scale 3D geological variation as encountered in the geothermal wells and the measured velocities of these formations. Most of the variation in the 3D starting model is due to the depth of the andesite, which varies between the two fields, and which has measured velocities of ~5 km/s versus ~3.5 km/s for the Tahorakuri Formation and similar volcaniclastic formations that overlie the andesite.

A coarse (3 x 3 x 0.5 km node spacing in the area encompassing the seismometers) and then finer (1.5 x 1.5 x 0.25 km node spacing) inversion grid was used for each of the three models with the final model from the coarse

inversion being used as the starting model for the finer grid inversion. In all cases the inversions were set to run for a

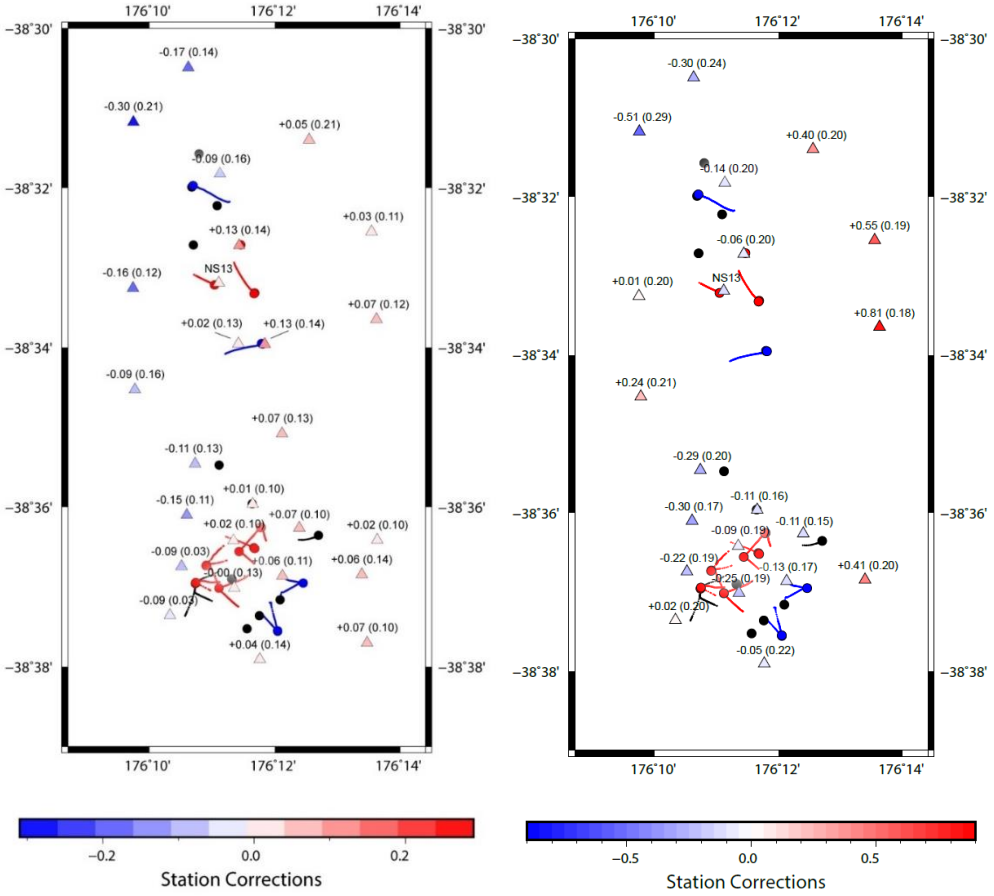

Figure 10. Mean station correction terms from all 1000 models for (a) Vp and (b) Vs for the main stations used in the Monte Carlo VELEST. Values are relative to NS13 which is close to the centre of the array and has been operating since early 2013. Red circles and lines and blue circles and lines show the production and injection wells resepectively.

maximum of 9 iterations, however all models ceased iterations due to the f-test indicating insignificant improvement in the data fit between iterations. All three of the models reached similar final RMS residual values of ~0.13 s (Table 1).

Table 1. Final RMS residuals (s) for the coarse and fine grids for all three models with the number of iterations in brackets.

	1D checkshot-logs	**1D VELEST**	**3D**
Coarse grid	0.14 (7 iters)	0.18 (4 iters)	0.14 (6 iters)
Fine grid	0.13 (2 iters)	0.13 (6 iters)	0.13 (2 iters)

3.3.2. Final models

Plotting of the diagonal element of the resolution matrix, a relative measure of how well the data constrains each inversion node, shows that high relative resolution is obtained between the events at depths between 1 to 2 km bsl (**Error! Reference source not found.**).

Absolute final velocity values for the three starting models varied substantially, possibly indicating that absolute velocity values are less well constrained than the relative velocity variation between areas. Velocities in the Rotokawa area were variable between the three models which suggests velocity structure in this area is not well determined by the available dataset and the inversion used here. Relatively low resolution values over the wider area at Rotokawa (**Error! Reference source not found.**), which in turn is due to source-receiver distribution in the area, supports this.

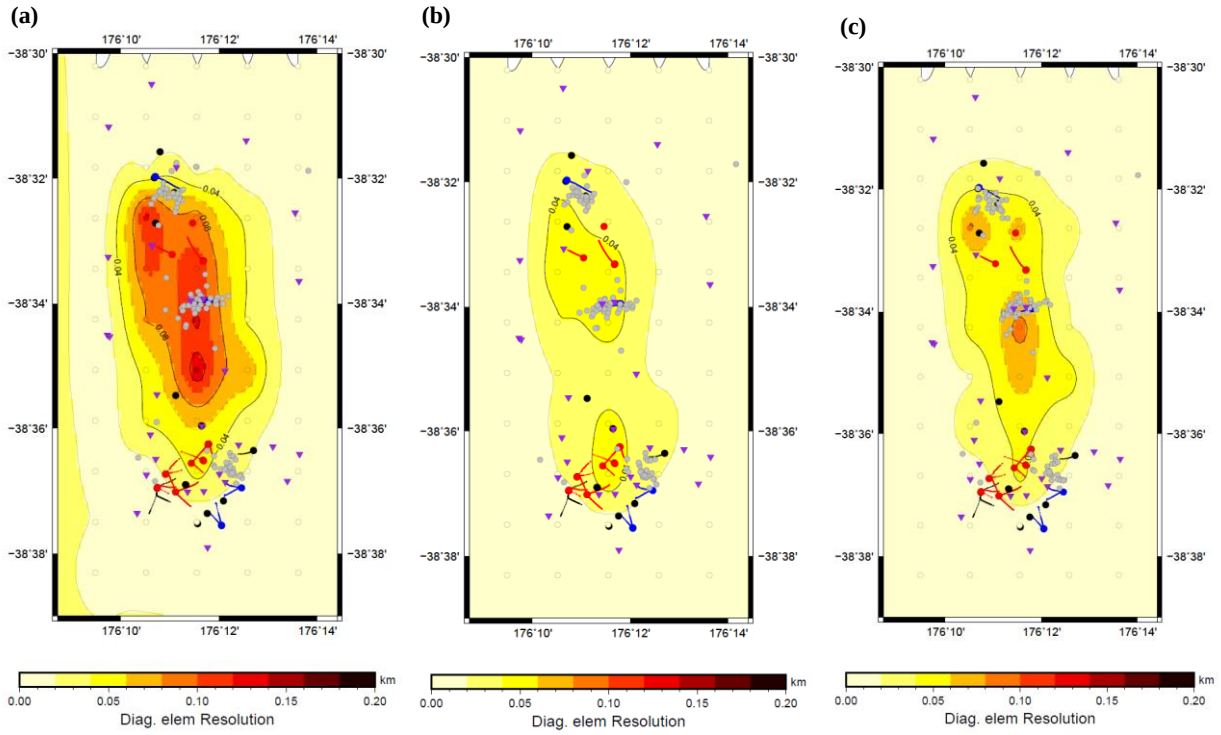

Figure 11. Diagonal element of the resolution matrix for the Vp model at 1.5 km depth for the three different starting models – (a) the 1D checkshot-log model (b) the 1D VELEST average model and (c) the 3D geology model. Hypocentre locations are shown as grey dots, seismometers as purple triangles and production and injection wells as red and blue circles and lines respectively. Inversion nodes are shown as grey unfilled circles.

All three final Vp models show a high-low velocity contrast occurring in the north of Ngatamariki between ~1 and 2 km bsl with the transition occurring approximately near the injection wells. The contrast appears to strike approximately north-south to northeast-southwest with higher velocities to the north and northwest. The location of the faster velocity agrees well with the VELEST station corrections, which also suggest faster velocity in the north and northwest (**Error! Reference source not found.**a). Resolution values in this area are however variable (**Error! Reference source not found.**), which suggests that although a contrast in velocity is apparent, the location of the contrast may not be particularly well constrained by the current distribution of sources and receivers.

The three final Vs models all show a low velocity region to the east of Ngatamariki and relatively high Vs to the north-west of Ngatamariki. The pattern is similar to that implied by the VELEST Vs station corrections (**Error! Reference source not found.**b).

3.3.3. Synthetic testing

Synthetic testing of the recovery of velocity variations was conducted in order to assess the spatial resolution of the current array and to assess the resolution improvement from adding 30 additional seismometers to the array in different configurations. The synthetic models used the Monte Carlo VELEST average as the 'base model' which is likely the most representative of velocity from 1.0 to 2.0 km bsl across the Ngatamariki and Rotokawa area. A high velocity region was included in the north of Ngatamariki from 0.5 to 2.0 km bsl (Vp = 4.5 km/s, +1 km/s compared to the base values) to represent the low porosity, silicificed/altered Tahorakuri Formation. A low velocity region was added in the production area at Rotokawa from 0.5 to 2.0 km bsl (Vp = 2.5 km/s, -1 km/s compared to surrounding) to simulate the possible effect of steam at the top of reservoir. From this velocity model, synthetic traveltime data were created for the current seismometer array (as at the end of 2016) and three different station spacings, 'high', 'medium' and 'low', for the 30 additional seismometers. The different station spacings were tested to see whether closer station spacing over the main anomalies of interest provided better spatial resolution in those regions. The synthetic data was created using the hypocentres from the 124 events used in the preliminary 3D inversion. The synthetic traveltime dataset included a +/- 200 m uncertainty in the hypocentres and a 0.2 s traveltime uncertainty that were randomly assigned from a triangular distribution to all phases picks. These uncertainties are similar to uncertainties observed in the existing dataset. The synthetic traveltime datasets were then inverted using the same inversion parameters as in the preliminary 3D tomography. All of the inversions achieved similar final rms residual values of ~0.08 after 9 iterations.

All four of the synthetic tests partially recovered the velocity variations but varied significantly in their ability to accurately recover their locations (**Error! Reference source not found.**). In all cases, the magnitude of the velocity anomalies recovered were smaller than the input velocity anomalies. Testing for the existing array does show some recovery of the high and low velocity regions, but the spatial recovery is poor. Similar results are apparent for the medium and high station spacing of the additional seismometers. The best recovery of the high and low velocity regions was obtained for the 30 additional seismometers at low density station spacing. This result suggests that obtaining ray path coverage across the study area is preferable to having very dense ray path coverage over the main areas of interest. The location of 30

additional seismometers that were deployed in March, 2017 were accordingly spread over the entire study area.

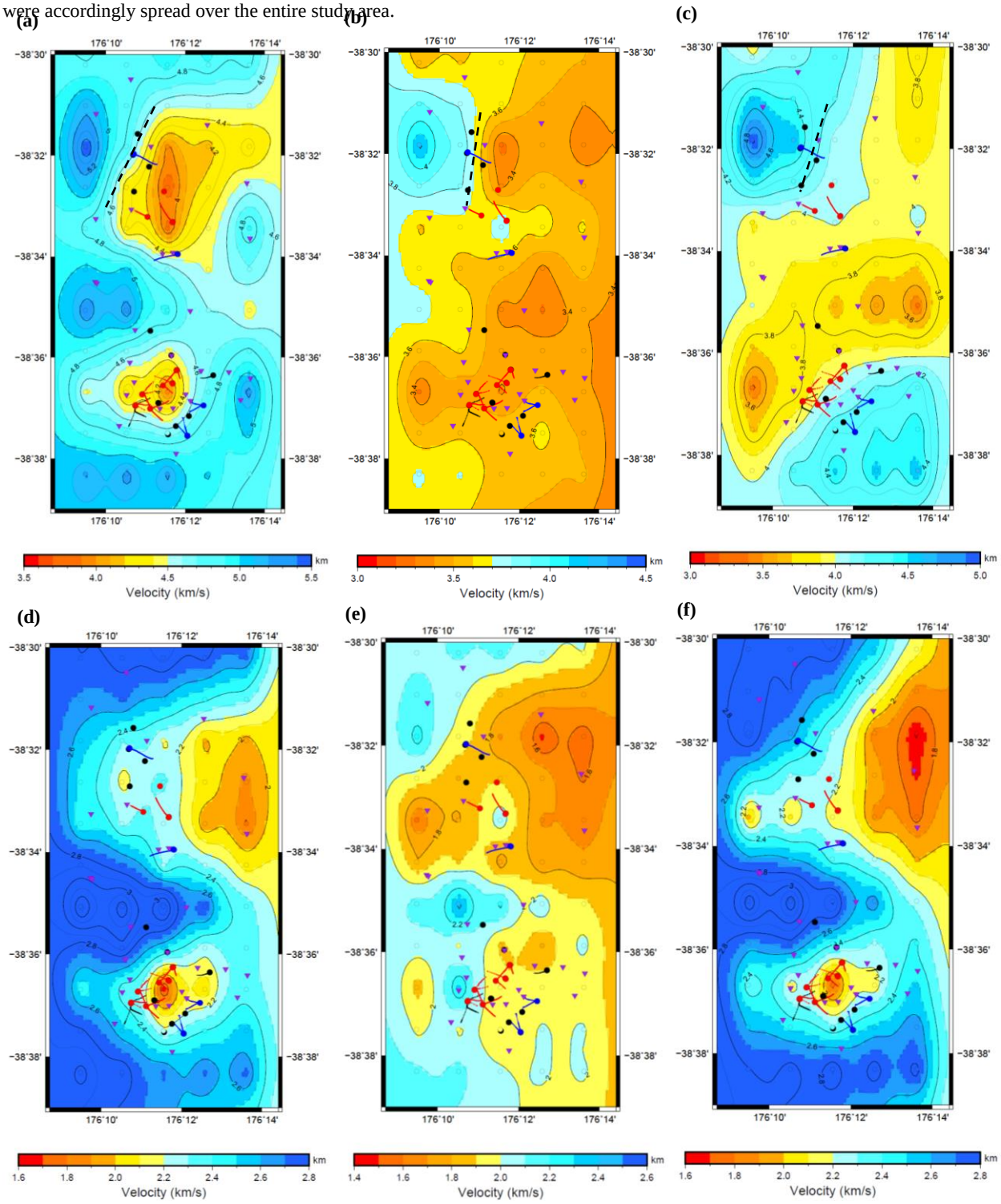

Figure 12. Slice of the Vp (a)-(c) and Vs (d)-(f) model at 1.5 km bsl for the three different starting models – (a) and (d) the 1D checkshot-log model (b) and (e) the 1D VELEST average model and (c) and (f) the 3D geology model. The dashed black line on the Vp models indicates the location of the high-low velocity contrast that is seen in all three models. N.B. different colour scales are used for each model.

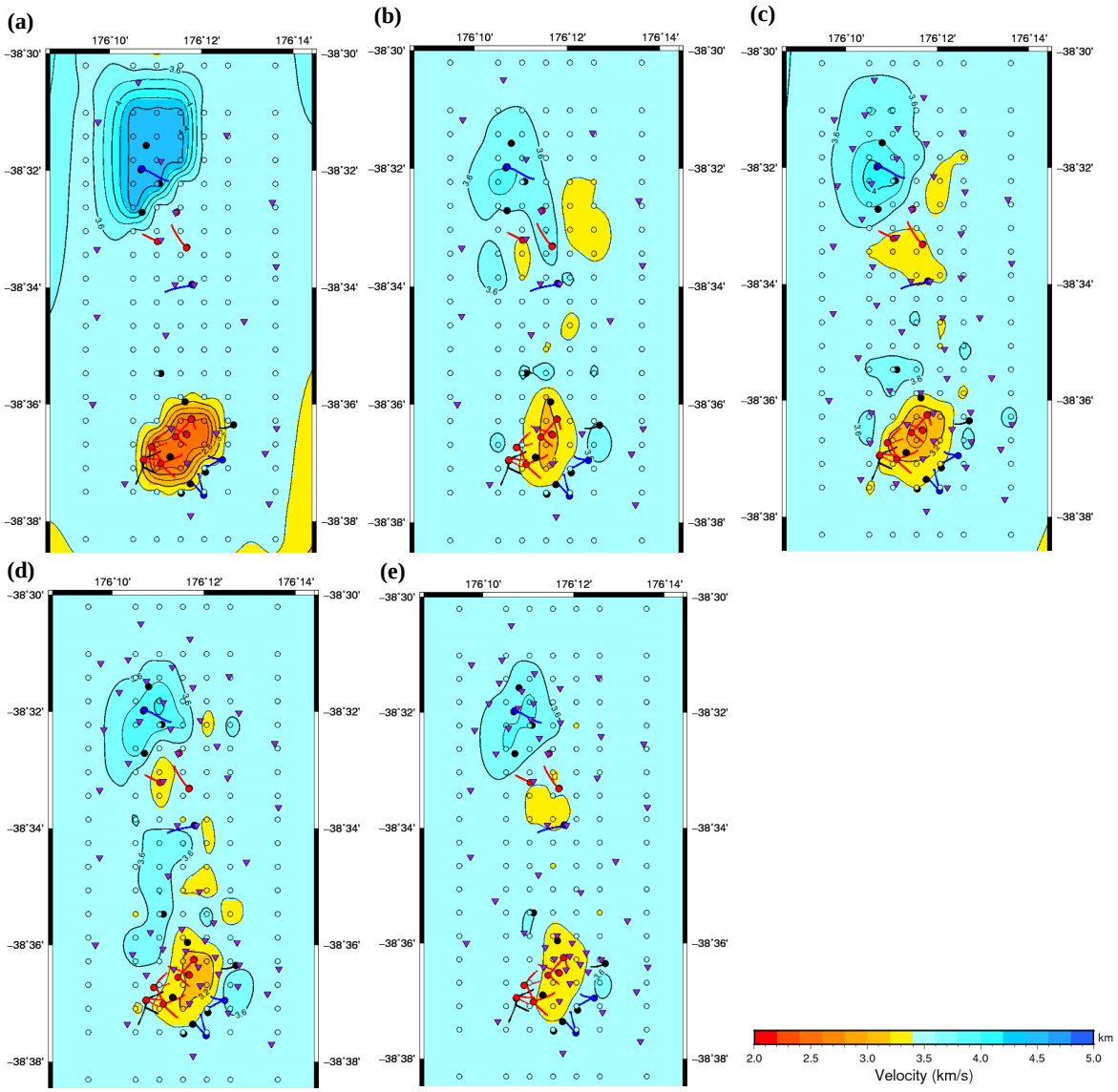

Figure 13. Synthetic testing results at 1.5 km bsl showing: (a) the input model; (b) recovery with the current stations; and recovery with 30 additional seismometers at (c) low density, (d) medium density and (e) high density station spacings. Open circles show the location of the inversion nodes.

4. DISCUSSION

The NM9 and NM10 logs show a large contrast in rock properties for the Tahorakuri Formation that is likely due to intense magmatic-hydrothermal alteration above an intrusive in NM9. Seismic velocity (Vp) is on average ~1 km/s faster and porosity on average ~10% lower in NM9 within the same tuff-dominated, Tahorakuri Formation. Velocity is particularly high (average of ~5 km/s) and porosity particularly low (average of ~ 2-3%) from ~2530 m depth to ~2940 m immediately above the intrusive complex in NM9. These values of seismic velocity are similar to those observed for andesite in NM10 and greywacke for KA52, with porosities similar to those observed within the intrusive itself. The differences observed between the Tahorakuri Formation in NM9 and NM10 show that intense alteration above intrusives within geothermal fields has the potential to drastically alter rock properties.

It is however currently uncertain whether the high-intensity silicification and lowering of matrix porosity seen in NM9 over the logging depths is present in the other wells in the north of the field. If silicification is not widespread, than the low-porosity and high velocity region may be smaller than currently anticipated, meaning it may not be the cause of low permeability. Chambefort et al. (2016b) do note however that phyllic alteration, characterized by deposition of silica, white mica and pyrite, is pervasive and widespread in the northern wells at Ngatamariki. Additional pXRF measurements are planned to investigate this.

The preliminary 1D and 3D tomography inversion work shows an apparent high-low contrast in seismic velocity (Vp and Vs) in the north of the Ngatamariki field. This appears to strike approximately NNW-SSE in the vicinity of NM9, with high velocity to the west of NM9 and low velocity to the east. This suggests the highly silicified, low

permeability Tahorakuri Formation does not extend to the east of the current northern injection wells.

However, the lack of high resolution values (and lower ray-path coverage) across the north and the synthetic testing of the current array suggest this feature is currently not well resolved spatially. Synthetic testing of an additional 30 seismometers placed across the current array shows a significant improvement in the spatial resolution of velocity variations within the two fields. It is therefore anticipated that the 30 seismometers deployed across the field in early 2017 will be sufficient to image the spatial extent of the high-velocity region apparent in northern Ngatamariki.

Both the Monte Carlo VELEST and the three different starting models used in the 3D inversion shows clearly the dependence of the final models on the starting models for this dataset. It will be important to continue to test this dependence in the on-going inversion work.

Further 3D inversion work will include double-difference tomography which offers improved resolution within the source (earthquake) region (Zhang and Thurber, 2007, 2003) using both the existing 2012-15 dataset and the 2017 dataset currently being acquired. Attenuation tomography will also be conducted.

2. CONCLUSION

A large contrast in seismic velocity (Vp ~Δ1 km/s) between north and south Ngatamariki within the Tahorakuri Formation is apparent from the sonic logs in NM9 and NM10. This appears to be due mostly to silicification associated with high intensity magmatic-hydrothermal alteration above an intrusion which has resulted in lower matrix porosity (~10% lower in NM9 compared to NM10) and hardening of the matrix frame. Since this alteration appears to be the cause of low permeability in the north of the field, imaging the high velocity associated with it via seismic tomography offers a potential way to map the low permeability in 3D. Preliminary 1D and 3D tomography inversions do show a high-low velocity contrast in northern Ngatamariki, however it appears that the current seismometer array at Rotokawa and Ngatamariki does not provide sufficient spatial resolution for mapping the high-velocity region at a field-scale. Synthetic testing shows that adding 30 seismometers across the array will significantly improve spatial resolution of the tomography.

ACKNOWLEDGEMENTS

We would like to thank the Rotokawa Joint Venture (Mercury and Tauhara North No.2 Trust) for access to the seismic and logging data used in this work and permission to publish. Mercury are thanked for financial support of the additional seismometer deployment. GNS Science, in particular Mark Simpson and Patti Durance, are thanked for allowing use of their pXRF and use of their facilities at Wairakei whilst conducting the pXRF measurements. Bill Cumming is thanked for his review and comments.

REFERENCES

Boseley, C., Cumming, W., Urzúa-Monsalve, L., Powell, T., Grant, M., 2010. A resource conceptual model for the Ngatamariki geothermal field based on recent exploration well drilling and 3D MT resistivity imaging, in: Proceedings World Geothermal Congress.

Chambefort, I., Buscarlet, E., Wallis, I.C., Sewell, S., Wilmarth, M., 2016a. Ngatamariki Geothermal Field, New Zealand: Geology, geophysics, chemistry and conceptual model. Geothermics 59, Part B, 266–280. doi:http://dx.doi.org/10.1016/j.geothermics.2015.07.011

Chambefort, I., Lewis, B., Simpson, M., Bignall, G., Rae, A., Ganefianto, N., 2016b. Ngatamariki Geothermal System: Magmatic to Epithermal Transition in the Taupo Volcanic Zone, New Zealand. Econ. Geol. In Press.

Chambefort, I., Lewis, B., Wilson, C.J.N., Rae, A.J., Coutts, C., Bignall, G., Ireland, T.R., 2014. Stratigraphy and structure of the Ngatamariki geothermal system from new zircon U–Pb geochronology: Implications for Taupo Volcanic Zone evolution. J. Volcanol. Geotherm. Res. 274, 51–70. doi:10.1016/j.jvolgeores.2014.01.015

Diehl, T., Kissling, E., 2009. Users Guide for Consistent Phase Picking at Local to Regional Scales.

Jaya, M.S., Shapiro, S.A., Kristinsdóttir, L.H., Milsch, H., Spangenberg, E., 2010. Temperature dependence of seismic properties in geothermal rocks at reservoir conditions. Geothermics 39, 115–123. doi:10.1016/j.geothermics.2009.12.002

Kissling, E., Ellsworth, W.L., Eberhart-Phillips, D., Kradolfer, U., 1994. Initial reference models in local earthquake tomography. J. Geophys. Res. Solid Earth 99, 19635–19646.

Rawlinson, N., Pozgay, S., Fishwick, S., 2010. Seismic tomography: a window into deep Earth. Phys. Earth Planet. Inter. 178, 101–135.

Rawlinson, N., Sambridge, M., 2003. Seismic traveltime tomography of the crust and lithosphere. Adv. Geophys. 46, 81–199.

Sewell, S.M., Cumming, W., Bardsley, C.J., Winick, J., Quinao, J., Wallis, I.C., Sherburn, S., Bourguignon, S., 2015. Interpretation of microseismicity at the Rotokawa Geothermal Field, 2008 to 2012, in: World Geothermal Congress 2015. p. 25.

Sherburn, S., Sewell, S.M., Bourguignon, S., Cumming, W., Bannister, S., Bardsley, C., Winick, J., Quinao, J., Wallis, I.C., 2015. Microseismicity at Rotokawa geothermal field, New Zealand, 2008–2012. Geothermics 54, 23–34. doi:10.1016/j.geothermics.2014.11.001

Thurber, C., Ritsema, J., 2007. Theory and Observations – Seismic Tomography and Inverse Methods, in: Treatise on Geophysics. Elsevier, pp. 323–360. doi:10.1016/B978-044452748-6.00009-2

Thurber, C.H., 1983. Earthquake locations and three-dimensional crustal structure in the Coyote Lake Area, central California. J. Geophys. Res. 88, 8226. doi:10.1029/JB088iB10p08226

Wallis, I., McCormick, S., Sewell, S., Boseley, C., 2009. Formation assessment in geothermal using wireline

tools-application and early results from the Ngatamariki Geothermal Field, New Zealand, in: Proceedings of the New Zealand Geothermal Workshop. Rotorua, New Zealand.

Wyering, L.D., Villeneuve, M.C., Wallis, I.C., Siratovich, P.A., Kennedy, B.M., Gravley, D.M., Cant, J.L., 2014. Mechanical and physical properties of hydrothermally altered rocks, Taupo Volcanic Zone, New Zealand. J. Volcanol. Geotherm. Res. 288, 76–93. doi:http://dx.doi.org/10.1016/j.jvolgeores.2014.10.008

Zhang, H., Thurber, C.H., 2007. Estimating the model resolution matrix for large seismic tomography problems based on Lanczos bidiagonalization with partial reorthogonalization. Geophys. J. Int. 170, 337–345. doi:10.1111/j.1365-246X.2007.03418.x

Zhang, H., Thurber, C.H., 2003. Double-Difference Tomography: The Method and Its Application to the Hayward Fault, California. Bull. Seismol. Soc. Am. 93, 1875–1889. doi:10.1785/0120020190